INTERNATIONAL JOURNAL FOR NUMERICAL METHODS IN FLUIDS
Int. J. Numer. Meth. Fluids **26**: 1181–1203 (1998)

EARLY STAGES OF AN IMPULSIVELY STARTED UNSTEADY LAMINAR FLOW PAST TAPERED TRAPEZOIDAL CYLINDERS

T.S. LEE

Mechanical and Production Engineering Department, National University of Singapore, Singapore 119260, Singapore

SUMMARY

Characteristics of the developing recirculation region behind a tapered trapezoidal cylinder and its interaction with the separating shear layer from the leading edges were studied numerically for an impulsively started laminar flow. An unsteady stream function–vorticity formulation was used. The Reynolds numbers considered range from 25 to 1000. Pressure contours, surface pressure coefficient, wake length and drag coefficient were studied through the streamline flow field. Main flow and subflow regimes were identified by an analysis of the evolution of the flow characteristics. It was found that typically, for a given trapezoidal cylinder, flow starts with no separation. As time advances, the symmetrical standing zone of recirculation develops aft of the trapezoidal cylinder. The rate of growth in width, length and structure of the aft end eddies depends on the Reynolds number. In time, separated flow from the leading edges of the trapezoidal cylinder also develops and forms growing separation bubbles on the upper and lower inclined surfaces of the trapezoidal cylinder. As time advances, the separation bubbles on the upper and lower inclined surfaces of the cylinder grow towards the downstream regions and eventually merge with the swelling symmetrical eddies aft of the cylinder. This merging of the flows creates a complex flow regime with a disturbed tertiary flow zone near the merging junction. Eventually, depending on the Reynolds number and the tapered angle of the trapezoidal cylinder, the flow develops into a specific category of symmetrical standing recirculatory flow with its own distinct characteristics. Comparisons with the available results of other investigators showed very good agreement. © 1998 John Wiley & Sons, Ltd.

KEY WORDS: trapezoidal cylinder; laminar flow; Reynolds number

1. INTRODUCTION

Studies of flow over cylinders are of great importance in many engineering applications, such as the design of tower structures, suspension bridges, chimneys, heat exchangers, road vehicles, tall buildings, flow meters etc. Most of the present work on flow over cylinders focused on long term flow development. Few considered using numerical methods in their studies on the early stages of impulsively started flow. The complexity of the early stages of impulsively started fluid flow meant that the accurate numerical computation of the flow field was very demanding. However, the evolution of the flow separation around cylinders at the early stages is very different from the long term wake development. Hence, the study of the flow development characteristics during the early stages of an impulsively started flow are necessary for a better understanding of the build-up of the recirculation zone before the flow burst into smaller Karman type of vortices.

CCC 0271–2091/98/101181–23$17.50

Received January 1997
Revised May 1997

Separated flow over bluff bodies such as circular cylinders, square cylinders, rectangular cylinders and flat plates has been studied by many researchers. However, few considered the trapezoidal cylinders. Davis and Moore [1] studied vortex shedding from two-dimensional time-dependent flow past rectangular cylinders. They noted that the build-up of fluid in the recirculation zones behind the body, prior to the initiation of shedding, caused large initial vortices, followed by some smaller and regularly shaped vortices which appeared when steady state shedding was reached. Nagano [2] investigated similar flow over a rectangular cylinder using the discrete vortex model instead of solving the Navier–Stokes equations with the finite difference or finite element method. Fernando and Modi [3] used a more sophisticated numerical approach—the boundary element method in conjunction with the discrete vortex model to represent the complex unsteady flow field around a bluff body with separating shear layers. Ling *et al.* [4] used a finite element method to investigate the Strouhal frequencies in vortex shedding over square cylinders with surface suction and blowing. Kim and Benson [5] made a comparison of various numerical methods: the SMAC, PISO and iterative time advancing schemes for unsteady flows past a circular and a square cylinder. The ability of each scheme to solve the unsteady flows was attributed to a pressure correction algorithm which strongly enforced the conservation of mass. For experimental work, many researchers studied the low Reynolds number flow around circular, rectangular and square cylinders. Bearman and Trueman [6] carried out a flow visualisation study of flow over rectangular cylinders. They showed that the drag coefficient was found to be strongly influenced by the presence of the trailing corners. Coutanceau and Bouard [7] and Bouard and Coutanceau [8] used flow visualisation as their main tool for studying the wakes behind an impulsively started flow past circular cylinders. They were interested in the near wake evaluation. They found that the characteristics of the pair of symmetric standing eddies and the appearance of secondary phenomena near the wake region depend on the initial Reynolds number. The characteristics of the early wake development can have a strong influence on the evaluation of the effects of secondary phenomena. Gerrard [9,10] carried out a series of experiments, including very careful flow visualisation studies on a circular cylinder in water using a towing tank. At a certain Reynolds number, the length of the recirculation region containing a pair of contra-rotating standing eddies was found to be approximately two cylinder diameters long. At higher Reynolds numbers, Gerrard observed dye which had rolled up into a votes returning towards the cylinder, in what he referred to as a 'finger'. Gerrard [10] also observed the three-dimensional nature of the wake flow, where the passage of time from the start of the motion showed the influence of the ends spread across the span, giving rise to bowed vortices. Okajima [11] and Okajima and Kitajima [12] investigated the fluid behaviour around square and rectangular cylinders in a wind tunnel and in a water tank. For the cylinders with width to height ratios of two and three, there existed a certain range of Reynolds numbers where the abrupt change of flow pattern occurred with a sudden discontinuity in the Strouhal number curves. For the Reynolds number below that region, the flow separated at the leading edges and reattached on either the upper or the lower surface during a period of vortex shedding. For Reynolds number above that region, the flow tended to reattach on the cylinder due to the increasing effects of the Reynolds stressed and turbulent entertainment at high Reynolds number. More recently, Kyoji and Yoshifumi [13] visualised water flow over a circular cylinder and a trapezoidal cylinder in a circular pipe, in order to investigate the complexity of the flow in a flow meter. From their experiment, it was shown that the formation of Karman vortex-like vortices is three-dimensional when they form behind a circular cylinder or a trapezoidal cylinder, as the separated shear layer wrapped up the fluid behind the cylinder. Also, the leading edge of the separation region was observed to move up to a certain distance behind the circular cylinder with the increasing Reynolds number.

2. GOVERNING EQUATIONS AND NUMERICAL PROCEDURES

Figure 1 shows the geometrical configurations of flow over a tapered trapezoidal cylinder. For the present study, the two-dimensional governing equations describing the flow over a trapezoidal cylinder are expressed as generalised streamfunction vorticity equations of the form

$$\frac{\partial \bar{\varsigma}}{\partial t} - \nabla \times (\bar{u} \times \bar{\varsigma}) = \frac{1}{Re} (\nabla^2 \bar{\varsigma}) + S, \tag{1}$$

$$\bar{\varsigma} = -\nabla^2 \bar{\psi}, \tag{2}$$

$$\bar{u} = \nabla \times \bar{\psi}, \tag{3}$$

where $\bar{\varsigma}$, $\bar{\psi}$, $\bar{u}$ represent the vorticity, stream function and velocity respectively, and S represents the source term. The inflow Reynolds number is defined as $Re = \rho u_0 b/\mu$.

For the solution domain considered, a uniform velocity is assumed at the inlet boundary. The normal derivative of the velocity is assumed to be zero at the outlet boundary. Along the other two horizontal boundaries, the flows are assumed to be sufficiently far from the influence of the square cylinder. Hence, the horizontal velocity component is assumed to be the undisturbed uniform velocity value and the normal velocity component is assumed to be zero. Non-slip conditions are applied at the surfaces of the square cylinder. The stream function and vorticity boundary conditions follow the relationships given by Equation (3) with respect to the specified velocity boundary conditions. The streamline at the axis of symmetry is assigned a reference value of zero.

The present work is concerned only with the initial stages of the impulsively started flow over the tapered trapezoidal cylinder. Thus, the numerical solution is an initial value problem. Besides the boundary conditions specified, the initial velocities, vorticity, pressure and stream-function fields must be known at the initial time. At time $t = 0$, the velocity field is assigned values at the inlet section (hence, the term 'impulsively started flow'). The initial pressure field is set to a reference value of zero.

In the present study, the flow governing Equations (1)–(3) is expressed in generalised curvilinear co-ordinate system. This allows the implementation of a numerical scheme on the

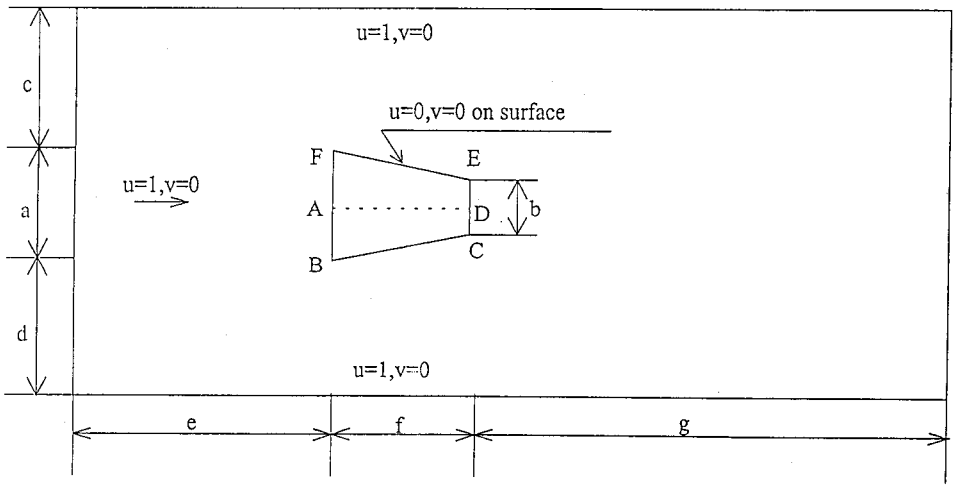

Figure 1. Problem definition of flow past a trapezoidal cylinder.

Cartesian grid, where the geometric characters are embedded in the coefficients of the transformed equations. The equations for any two-dimensional cross-sections are then obtained by specifying suitable coefficients for the transformed governing equations. All the transported properties are expressed in their conservative form.

For the two-dimensional problem considered here, the curvilinear velocity U, V and the Cartesian velocity components u, v are related by

$$U = u\xi_x + v\xi_y, \qquad V = u\eta_x + v\eta_y. \tag{4}$$

The Jacobian matrix J and the matrix terms ξ_x, ξ_y, η_x, η_y are obtained from

$$\xi_x = \frac{y_\eta}{J}, \qquad \xi_y = -\frac{x_\eta}{J}, \qquad \eta_x = -\frac{y_\xi}{J}, \qquad \eta_y = \frac{x_\xi}{J}. \tag{5}$$

The algorithm of the numerical solution is followed closely by the alternating direction implicit (ADI) method proposed by Samarskii and Andree [14]. The advancement over one time step is accomplished by:

$$\begin{aligned} &(I - \Delta t A_\varepsilon)(\bar{\varsigma})^* = (A_\varepsilon + A_\eta)(\bar{\varsigma})^n + (S_D)^n \\ &(I - \Delta t A_\varepsilon)(\bar{\varsigma})^{**} = (\bar{\varsigma})^* \\ &(\bar{\varsigma})^{n+1} = (\bar{\varsigma}) + \Delta t(\bar{\varsigma})^{**} \end{aligned} \tag{6}$$

The streamline field is then obtained from the vorticity field through Equation (2) by a successive over relaxation (SOR) iteration procedure [15]. The velocity fields are obtained from Equation (3) and the pressure field is obtained directly from the streamline field:

$$\nabla^2 P = 2\left[\frac{\partial^2\psi}{\partial x^2}\frac{\partial^2\psi}{\partial y^2} - \left(\frac{\partial^2\psi}{\partial x\,\partial y}\right)^2\right] \tag{7}$$

A hybrid difference scheme [16] implemented for the convection related terms is outlined as follows:

$$\frac{\partial\phi}{\partial r} = \frac{\phi_{i+1} - \phi_{i-1}}{2\Delta r}\,\omega + \frac{\phi_i - \phi_{i-1}}{\Delta r}\,(1-\omega)A + \frac{\phi_{i+1} - \phi_i}{\Delta r}\,(1-\omega)B, \tag{8}$$

where ϕ denotes the convection related transport parameters, r is ξ or η and i is the index of grid point. The parameters ω, A and B are determined by the local cell Reynolds number (Re_1) as follows:

$$\text{if } |Re_1| < 2.0, \quad \text{then} \quad \omega = 1.0, \quad \text{A} = 0.0, \quad \text{B} = 0.0, \tag{9a}$$

$$\text{if } |Re_1| \le 2.0, \quad \text{then} \quad \omega = 1.0, \quad \text{A} = 1.0, \quad \text{B} = 0.0, \tag{9b}$$

$$\text{if } |Re_1| \ge 2.0, \quad \text{then} \quad \omega = 0.0, \quad \text{A} = 0.0, \quad \text{B} = 1.0, \tag{9c}$$

where $Re_1 = u_\xi \cdot \Delta\xi \cdot Re$ or $u_\eta \cdot \Delta\eta \cdot Re$ for the convective terms in the ξ- or η-direction, respectively.

Second-order upwind schemes are used for the convection terms in the governing equation and the three-point central difference schemes are used for the diffusive terms. At the grid points adjacent to the boundary, central difference schemes are used for each variable. The details are described as follows.

The convection terms are discretised as:

$$u_\xi \frac{\partial \phi}{\partial \xi} = \begin{cases} u_{\xi_{i,j}} \dfrac{3\phi_{i,j} - 4\phi_{i-1,j} + \phi_{i-2,j}}{2\Delta\xi} & \text{if} \quad u_{\xi_{i,j}} \geq 0 \\ u_{\xi_{i,j}} \dfrac{-3\phi_{i,j} + 4\phi_{i+1,j} - \phi_{i+2,j}}{2\Delta\xi} & \text{if} \quad u_{\xi_{i,j}} < 0 \end{cases} \quad \text{for inner points,} \tag{10}$$

$$u_\eta \frac{\partial \phi}{\partial \eta} = \begin{cases} u_{\eta_{i,j}} \dfrac{3\phi_{i,j} - 4\phi_{i,j-1} + \phi_{i,j-2}}{2\Delta\eta} & \text{if} \quad u_{\eta_{i,j}} \geq 0 \\ u_{\eta_{i,j}} \dfrac{-3\phi_{i,j} + 4\phi_{i,j+1} + \phi_{i,j+2}}{2\Delta\eta} & \text{if} \quad u_{\eta_{i,j}} < 0 \end{cases} \quad \text{for inner points,} \tag{11}$$

and for points adjacent to the boundary,

$$u_\xi \frac{\partial \phi}{\partial \xi} = u_{\xi_{i,j}} \frac{\phi_{i+1,j} - \phi_{i-1,j}}{2\Delta\xi}, \tag{12}$$

$$u_\eta \frac{\partial \phi}{\partial \eta} = u_{\eta_{i,j}} \frac{\phi_{i,j+1} - \phi_{i,j-1}}{2\Delta\eta}. \tag{13}$$

The present work is concerned only with the initial stages of the impulsively started flow over a tapered trapezoidal cylinder. Therefore, the numerical solution of the impulsively started flow over a tapered trapezoidal cylinder is an initial boundary value problem. Apart from the boundary conditions specified earlier, the velocities and pressure must be known at the initial time, in order to carry out the numerical computation of the unsteady flow. The solution sequence for each flow condition is thus given by

1. At time $t = 0$, the velocity in the whole of the solution domain is given values at the inlet section (hence the term impulsively started flow). The initial streamline field and the vorticity fields are then calculated. The initial pressure field is set to a reference value of zero.
2. For $t > 0$, the vorticity equation is solved by the ADI and block TDMA [17] codes.
3. The streamline field is then obtained from Equation (2) through the SOR method.
4. The velocity and pressure fields are updated with the new streamline field obtained.
5. The information for pressure coefficients, drag coefficient, etc., are obtained from the pressure field. The wake length is estimated from the above solutions.

In the above computational procedures, the velocities at the corners of the square cylinder are undefined. Therefore, the conditions in these areas are treated separately. Here the multidomain iterative procedure is introduced, with the whole computational domain being divided into four subdomains and the sharp corners located at the boundary of each subdomain. This method simplifies the definition of boundary conditions at the sharp corners, because they are treated as a solid boundary of a subdomain when numerical iterations of the entire solution domain are obtained.

The boundary conditions are shown in Figure 1 and the finite difference mesh used in the present study are shown in Figure 2. The location of the cylinder in the computational domain as shown in Figure 1 is determined through a series of preliminary numerical test runs. For $b = 1/2a$, the optimum parameters determined are: $c = d = 7a$, $e = 4.5a$, $g = 14.5a$ and $f = a$, where a is the length of the frontal side of the trapezoid, and b is the length of the rear side. The distance from the symmetrical axis of the cylinder to the lower and upper sides of the computational domain is chosen to be sufficiently large, so that it satisfies the requirement that the solution domain is almost infinite. The finite difference mesh used is shown in Figure 2. Grid independent tests have been carried out for an impulsively started flow over a trapezoidal cylinder at $Re = 100$ on grid points of 81×61, 161×121 and 181×161. From the results obtained for

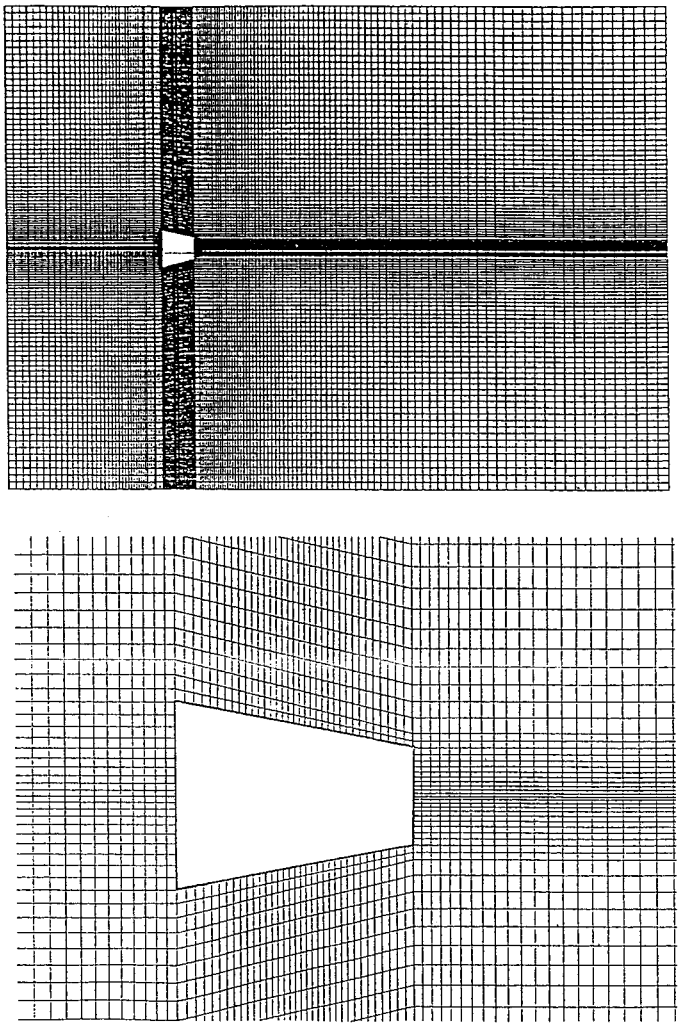

Figure 2. Finite difference mesh.

the wake length (Figure 3), the difference between these three grid sizes is negligible. Thus, the total number of grids used in the present calculation is 161×121. A numerical grid generation procedure was also introduced to provide more grid points near the solid boundary, to obtain a better insight of the fluid phenomena within the wake regions.

For the present analysis of the impulsively started flow over the tapered trapezoidal cylinders, numerical results are presented for time variations of streamline patterns, pressure contours, surface pressure coefficients, drag coefficients and closed wake length.

3. RESULTS AND DISCUSSIONS

The numerical results obtained for flow past a tapered trapezoidal cylinder at $Re = 25$, 50, 250, 500 and 1000 are presented for study of the early stages of symmetrical wake flow develop-

ments. Computations of the symmetrical flow past the tapered trapezoidal cylinder were obtained up to a dimensionless time of $t = 8$.

Figures 4–9 show the evolution with time of the impulsively started streamline flow structure over the tapered trapezoidal cylinder for $Re = 25$, 50, 150, 250, 500 and 1000, respectively. Immediately after it starts, the flow is typically irrotational everywhere (Type I main-flow). But as the flow moves over the tapered trapezoidal cylinder, vorticity is generated at the solid surface and transported to the region of the rear stagnation point, inducing a reverse flow. This reverse flow grows in time into a symmetrical standing zone of recirculation at the aft end of the cylinder (Type II main-flow). Flow separation from the leading edges of the tapered trapezoidal cylinder also develops as Re increases or when time advances (Type III main-flow). Above a critical Reynolds number Re_{crit}, and after a critical period of time (t^*) which is shorter for greater Reynolds numbers, the separated flows from the leading edges of the tapered trapezoidal cylinder merge with the swelling recirculation wake flow region at the aft end of the cylinder. This creates a complex recirculatory flow pattern (Type IV main-flow) with possible tertiary recirculations at the meeting points of the Type II and Type III separated flows. However, the present investigation is limited to cases where the recirculation zones in which eddies develop remain symmetrical and stably attached to the tapered trapezoidal cylinder.

A simple qualitative examination of the contours of the developing streamlines shows that the time development of the flow differs when Re is increasing. It is possible to distinguish three categories of flow time evolution which correspond roughly to small, moderate and high Reynolds numbers, while the flow remains symmetrical and attached to the tapered trapezoidal cylinder:

$$Re < Re_1, \qquad Re_1 < Re < Re_2 \quad \text{and} \quad Re > Re_2.$$

The exact limiting values of Re_1 and Re_2 cannot be determined by this qualitative investigation; they will be classified subsequently by means of the numerical presentations of the streamline contours on the main characteristics of the flow. However, for the sake of illustration, it can be said that the values of Re_1 and Re_2 have been found to be approximately 25 and 150.

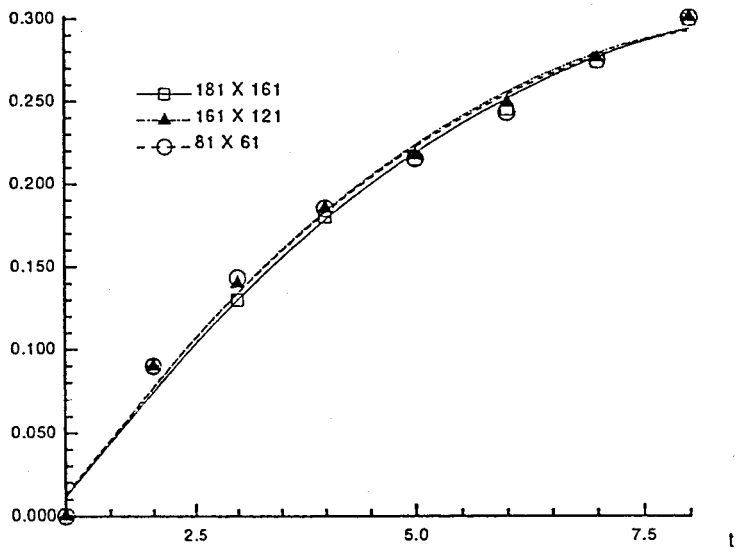

Figure 3. Test on the effect of grid point number (comparison of wake lengths).

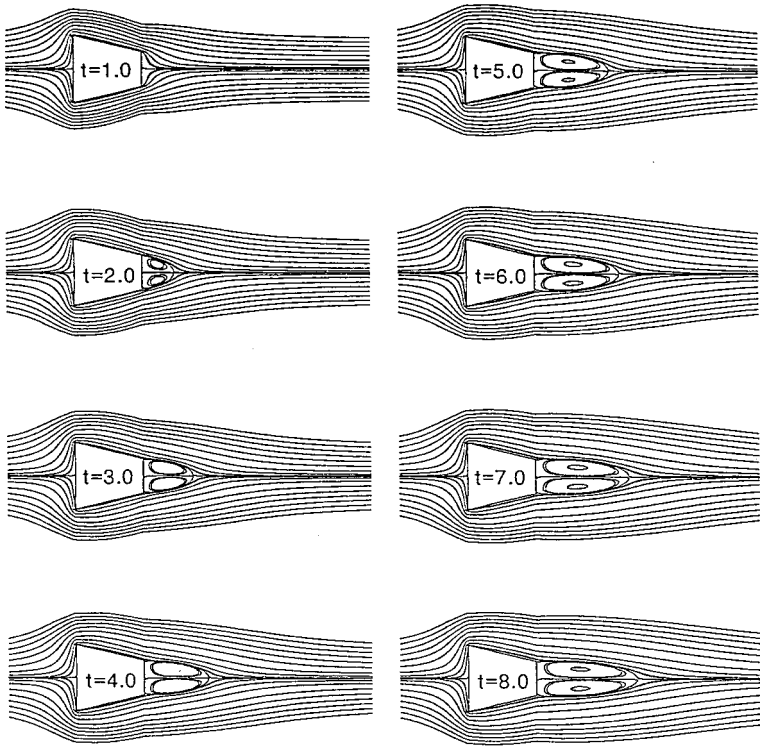

Figure 4. Instantaneous streamline pattern for $Re = 25$ at various times.

3.1. Time evolution at low Reynolds numbers: $Re < Re_1$

If the value of Re remain below a certain limiting value of Re_1 and the flow time is small ($t < 1.0$), the flow develops with time without visible flow separation and reattachment (Type I main-flow). After a short lapse of time, the flow separates first from the rear surface of the tapered trapezoidal cylinder (Type II main-flow) and forms aft end symmetrical eddies within a recirculating zone (subflow (a)). This unique recirculating zone typically consists of the two symmetrical eddies. For $Re \approx 25$ the twin eddies occur as soon as $t > 1.5$. The length and the width of the recirculation region increase as flow time advances. However, the width of the recirculation region remains smaller than the width of the aft end of the tapered trapezoidal cylinder.

3.2. Time evolution at moderate Reynolds numbers $Re_1 < Re < Re_2$

As the Reynolds number is further increased, the domains of the recirculating zone increase rapidly. Recirculatory flow phenomena begin to appear during the flow development, which is typical for this category of flow. First, the fluid particles passing through the region near the sharp corners at the rear surface of the tapered trapezoidal cylinder deviate from the cylinder, causing a separation region in the streamline pattern. The recirculation region of the close wake is established. As flow time progresses, streamlines separating from the leading edges of the upper and lower inclined surfaces of the tapered trapezoidal cylinder (Type III main-flow) merge with the growing recirculation region at the aft end of the cylinder. This results in a complex recirculatory flow pattern (Type IV main-flow) with tertiary recirculations (subflow

(c)) near the meeting points between the Type II and Type III flows. The complexity of the flow pattern depends on the Reynolds number. The width of the recirculation region is now slightly larger than the width of the aft end of the tapered trapezoidal cylinder.

For $Re = 50$, Figure 5 shows that at $t < 1.0$, there is no observable flow separation over the leading edges of the tapered trapezoidal cylinder. For $t > 1.0$, flow separations begin at the trailing edges of the tapered trapezoidal cylinder. The twin eddies can be seen issuing from the rear stagnation point of the cylinder. For $t > 3.0$, the separated flow region grows in size and development of the symmetrical eddies can be seen through the corresponding streamline pattern behind the tapered trapezoidal cylinder.

3.3. Time evolution at high Reynolds numbers, $Re > Re_2$

Beyond the limiting value of Re_2, two different sorts of phenomena occur which complicate the time development of the flow. As seen from Figures 6–9, after a certain lapse of time following the impulsively started flow over the tapered trapezoidal cylinder, the upper and lower surface shear layers begin to merge with the main recirculating zone at the aft end of the square cylinder, thus creating disturbances (subflow (c)) at the point of merging.

For $Re = 150$ and $t > 1.0$, the twin eddies appear nearer to the rear corners instead of at the centre of the aft surface of the tapered trapezoidal cylinder. At $t = 3.0$, the streamlines separate at the leading corners of the tapered trapezoidal cylinder, forming recirculatory flow regions at the upper and lower inclined surfaces of the cylinder. As time advances, these separated secondary flows move towards the rear end and join up with the recirculating flow in the wake region. A tertiary subflow region was identified.

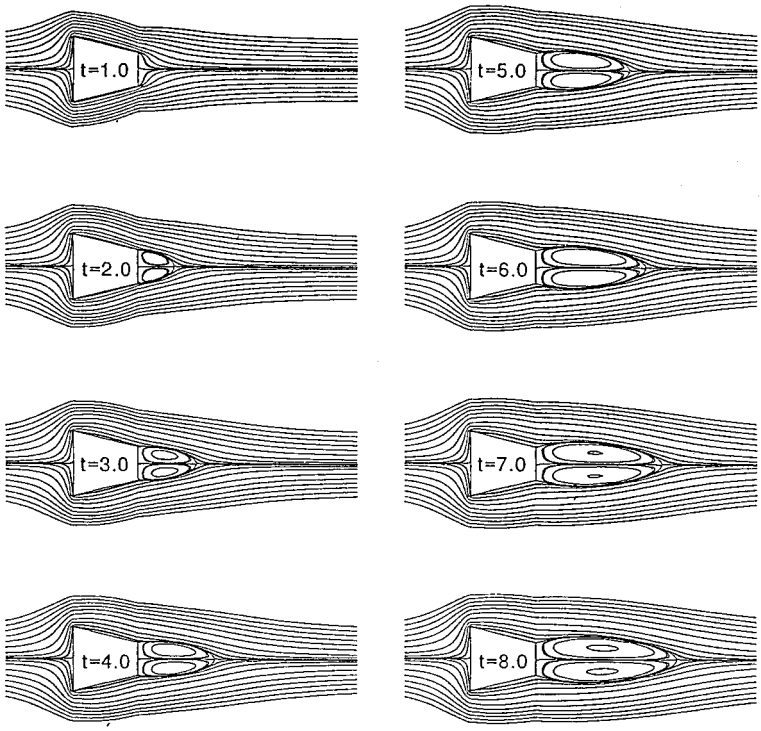

Figure 5. Instantaneous streamline pattern for $Re = 50$ at various times.

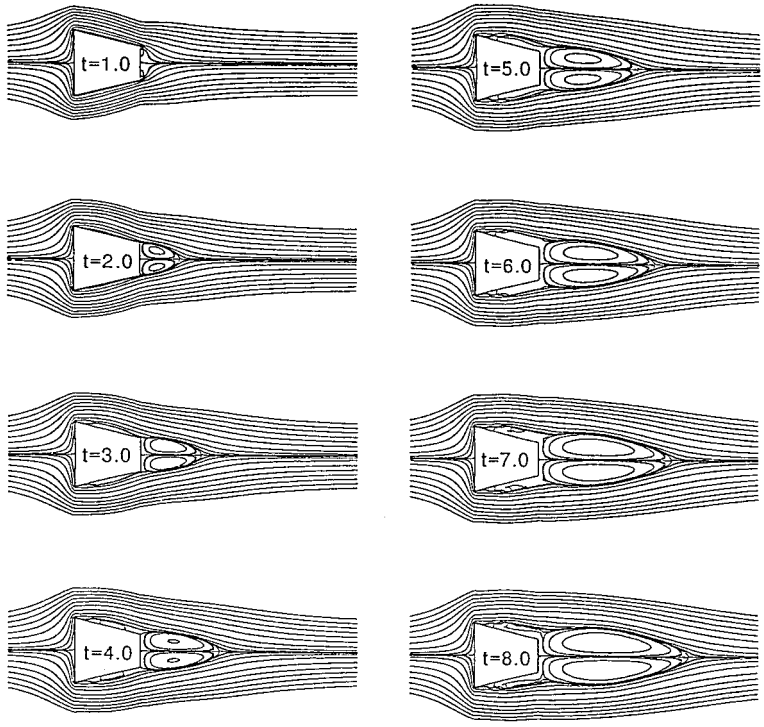

Figure 6. Instantaneous streamline pattern for $Re = 150$ at various times.

For $Re = 250$, 500 and 1000, the sizes of the twin eddies at $t > 5$ are observed to be almost similar at the corresponding time levels for these flows. However, the sizes of the separated shear layer at the upper and lower inclined surfaces of the tapered trapezoidal cylinders are larger for higher Reynolds number at the corresponding time level. Thus, for a corresponding time level, higher Reynolds numbers will give a larger combined recirculatory flow region and a more obvious tertiary recirculatory flow regime.

It should be pointed out here that for larger values of t, if an external disturbance is introduced, this will lead to vortex shedding. The flow solution may then bifurcate between symmetrical wake and Karman wake. It is also possible that the symmetrical wake at higher Reynolds numbers bifurcates between a steady state configuration and oscillating configuration or a periodic one of different nature. These are not within the present scope of study.

3.4. Evolution of the flow characteristics in the subflow regions

Figures 4–9 also show the time evolution of the shape and structure of the various type of subflows (a) (b) and (c) for different values of the Reynolds number. The recirculation eddies at the aft end of the cylinder (subflow (a)) rotate in the same directions as the eddies at the upper and lower inclined surfaces of the tapered trapezoidal cylinder (subflow (b)). The flow separation shear layers and the main recirculation zone grow in size with time and as Reynolds number increase.

For $Re = 25$, Figure 6 shows the typical time development of the subflow (a). It starts from the rear cylinder surface without presenting any variation in the concavities and remains smooth until the downstream extremities. It can be seen that in the earlier stage of the flow

development the point of reattachment moves very quickly downstream. But from $t > 3.0$ the evolution becomes slow. At this value of Re, the maximum width of subflow (a) remains, at most, equal to the width of the trailing edge of the tapered trapezoidal cylinder.

For $Re = 50$, the outlines of the subflow (a) closely follow that for $Re = 25$ and $t < 3.0$. The width of the wake remains smaller than the width of the trailing edge of the tapered trapezoidal cylinder. But for $t > 3.0$, the width of the wake becomes slightly larger than the width of the trailing edge of the tapered trapezoidal cylinder.

For $Re = 150$, 250, 500 and 1000, the width of the wake of subflow (a) clearly becomes larger than the width of the trailing edge of the tapered trapezoidal cylinder for $t > 3.0$. The separated flows (subflow (b)) developing from the leading edges of the cylinder begin to merge with the recirculation zone in the wake region. For $t > 6.0$, however, the size of the recirculation zone remains similar to that where $Re = 150$, 250, 500 or 1000.

In general, the above study shows that for Reynolds number greater than a critical value and after a certain time period, separated flows from the leading edges of the tapered trapezoidal cylinder merge with the growing main recirculating zone aft of the cylinder. This creates a tertiary flow regime (subflow (c)) between the two merging recirculatory flows.

3.5. Evolution of other characteristics

Having made a comprehensive study by analysing the characteristics of the main recirculatory flow regions, the other derived characteristics of the flow, viz. the flow field pressure contours, the surface pressure coefficient, the wake length and the drag coefficient are considered.

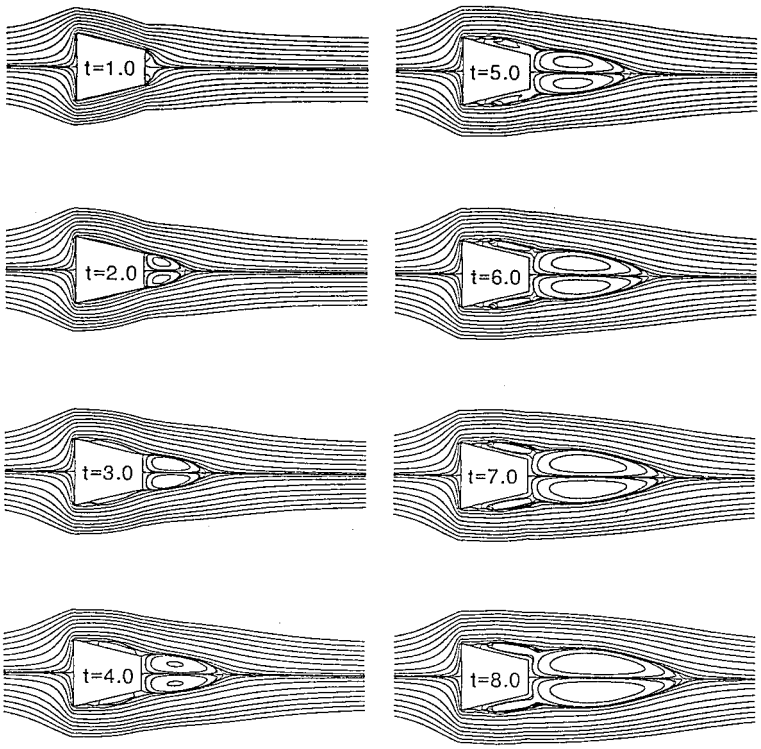

Figure 7. Instantaneous streamline pattern for $Re = 250$ at various times.

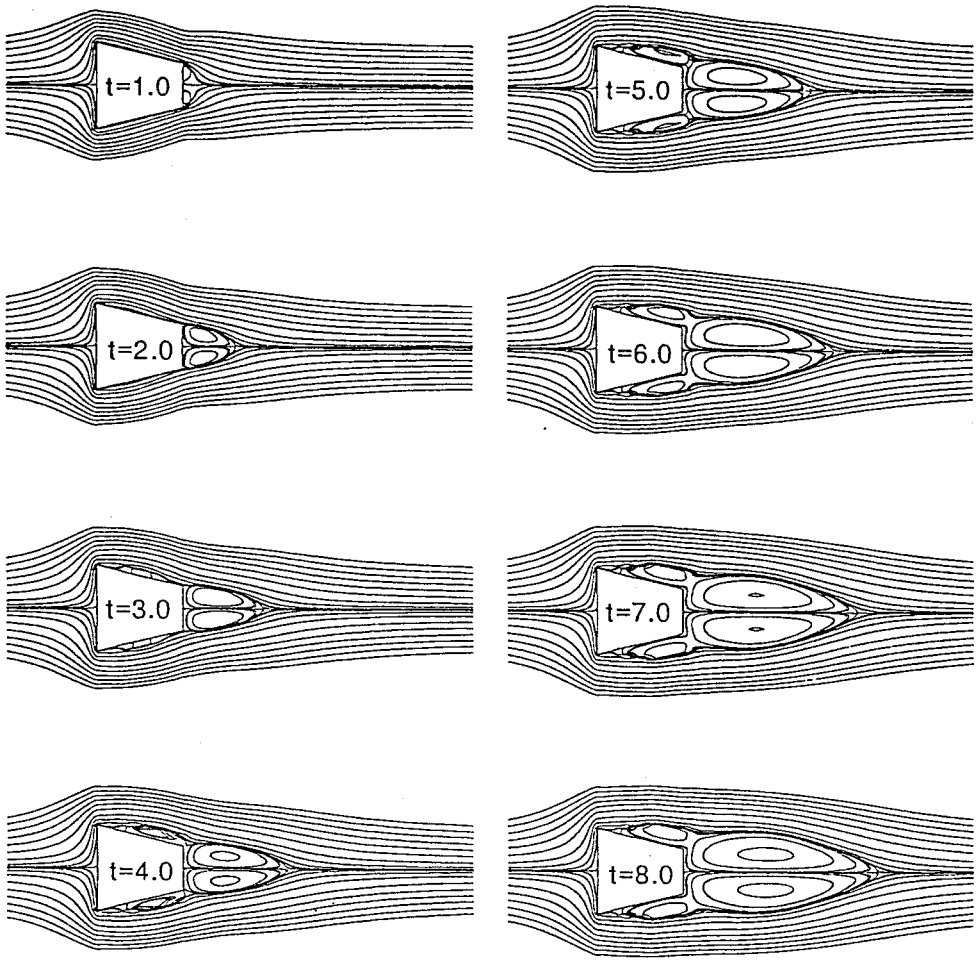

Figure 8. Instantaneous streamline pattern for $Re = 500$ at various times.

Figures 10–15 show the time variation at $t = 2.0$, 4.0, 6.0 8.0 and 10.0 of the pressure contours for $Re = 25$, 50, 150, 250, 500 and 1000, respectively. For the range of Reynolds numbers considered here, the development of the pressure contour lines closely follow the development of the streamline patterns. For $Re = 25$ and $t = 2.0$, the pressure contour indicates that there is little recirculation region present. As time advances, the development of the wake region behind the rear wall of the tapered trapezoidal cylinder is recognised. From the corresponding streamline patterns for $Re = 50$, the small vortices can be seen to develop from the rear wall causing the pressure contour lines to separate at $t = 2.0$. The pressure contour lines become closer and eventually merge at $t = 8.0$. From the outline of the wake region at different time levels, the twin vortices can be seen growing larger with increasing time. Figure 12 shows the pressure contours for $Re = 150$. In comparison with the pressure contours for $Re = 25$ and 50, the outline of the wake region from the frontal corners to the rear stagnation point is larger. From the previous study of the streamline patterns, secondary recirculation is known to develop at these corresponding Reynolds numbers. However, the variations in the pressure contours are not significant when the recirculation regions are fully developed. For

higher Reynolds numbers (Figures 13–15), the pressure contours become more complex. Separation flow at the frontal corners merges with the recirculation region at the aft end as time advances. The development of the symmetrical eddies at the aft end of the cylinders can be observed from the changes of the pressure contours in the trailing wake region. For $Re < 50$, the recirculation pattern behind the cylinder is small. For $Re > 250$, the pressure contours show a complicated pattern compared with that of the lower Reynolds numbers of $Re = 25$ and 50. At $Re = 250$, the secondary recirculation region at the upper and lower inclined surfaces of the cylinder can be seen to merge with the wake region aft of the cylinder, forming a single tertiary recirculating flow region between the separated flow from the leading edge and the recirculation region at the aft end of the cylinder.

Figures 16 and 17 show the distributions of surface pressure coefficients ($Cp = (p - p_\infty)/(0.5\rho u_\infty^2)$) at various times for $Re = 50$ and 500, respectively. Interesting flow features can be observed from these surface pressure coefficients. The surface pressure coefficients at the frontal stagnation point have the maximum positive value. The minimum Cp (negative value) appears on the surfaces of the inclined side immediately after the frontal corners. The changes of the surface pressure coefficients are gradual along the two inclined side walls of the cylinder.

In this study, the wake length is defined as the distance between the downstream stagnation point on the symmetric axis and the cylinder rear surface. Figure 18 shows the time variation of the wake length with time at various Reynolds numbers. At $Re = 25$, the rate of the time variation of wake length is slower than other Reynolds numbers. For $Re > 50$, the wake length increases almost linearly with time. The figures show that at the same time instant, the wake length increases very little with the increasing Reynolds numbers considered here.

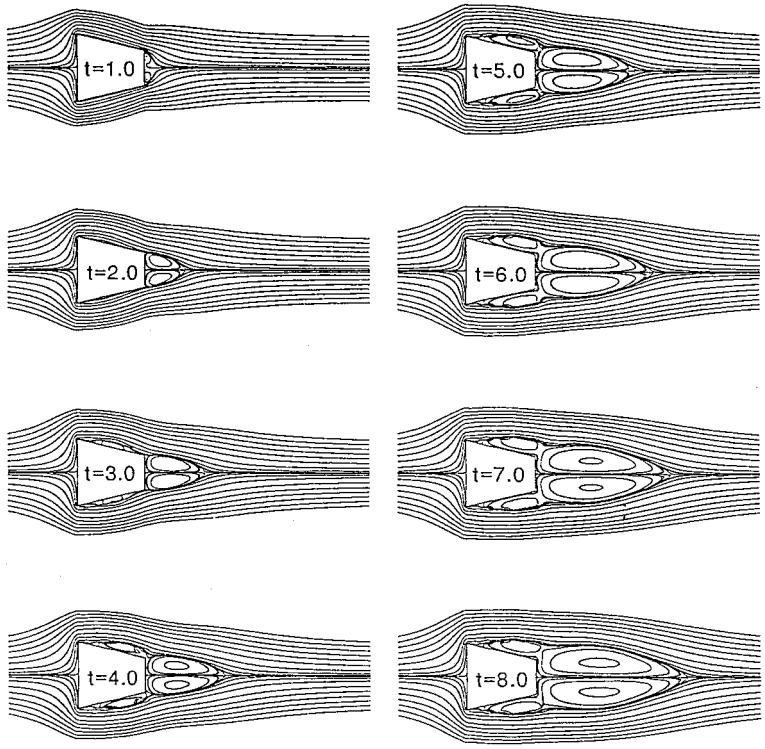

Figure 9. Instantaneous streamline pattern for $Re = 1000$ at various times.

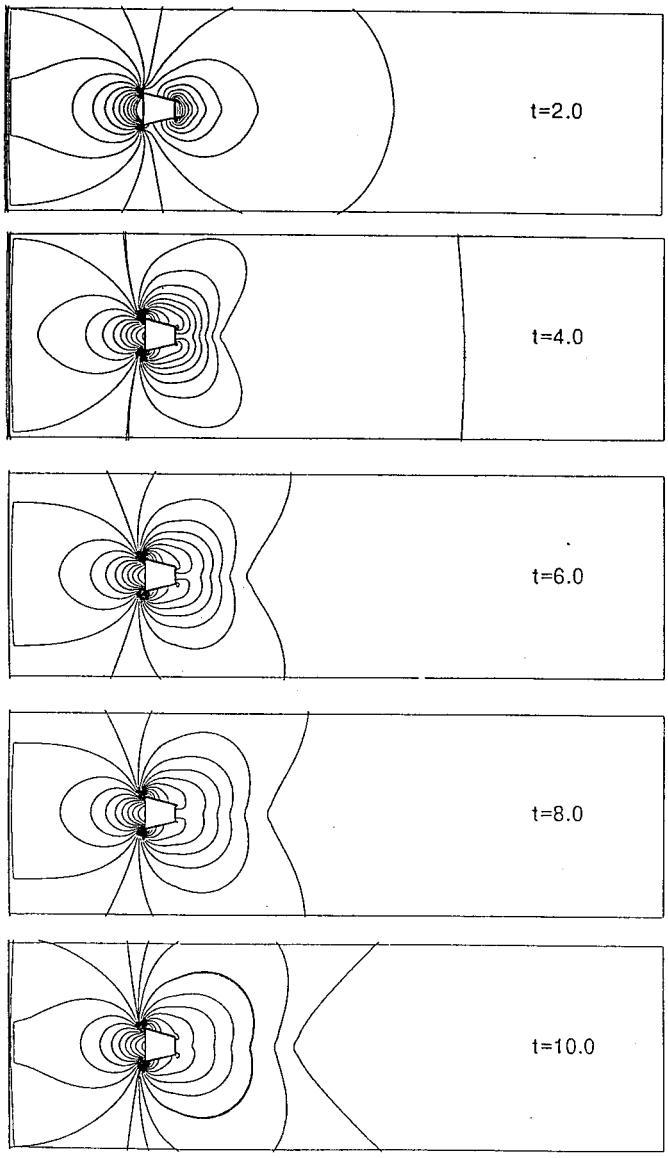

Figure 10. Time variation of the pressure contours at $Re = 25$.

Figure 19 shows the variation of drag coefficients (Cd) with time for various Reynolds numbers. At low Reynolds numbers, the Cd variations are different from those at high Reynolds numbers. For $Re > 150$, there are no obvious difference in the variation of the drag coefficients. For $Re = 25$, the drag coefficient drops rapidly from the maximum value. As the time advances, Cd varies in a narrow range and the magnitude of that range becomes smaller, until finally, after $t = 17.0$, it approaches a value of ≈ 1.70. This is smaller than the corresponding case for the square cylinder ($Cd = 2.0$) under the same flow condition. The Cd-curve for $Re = 50$ shows similar behaviour. The value is much smaller compared with the case of $Re = 25$. It approaches a value around 1.61 as time advances. For Reynolds numbers

between 150 and 1000, the *Cd* curves are similar and the differences between them are small. The drag coefficients decrease rapidly from $t = 1.0$ to 5.0 and then increase after $t = 5.0$. They soon decrease again at $t = 9.0$ and eventually approach $Cd = 1.50$ at $t = 18.0$. The maximum *Cd* values appear at the beginning of the impulsively started flow over the tapered trapezoidal cylinder. The initial *Cd* values fluctuate due to the creation of secondary recirculation flow patterns and their changes with respect to time during the initial development stages of the impulsively started flow. At first, only the twin vortices appear at the wake region behind the rear wall of the cylinder. The drags decrease from the initial maximum value. When the secondary recirculation is initiated, the drag will increase during the developmental stages of

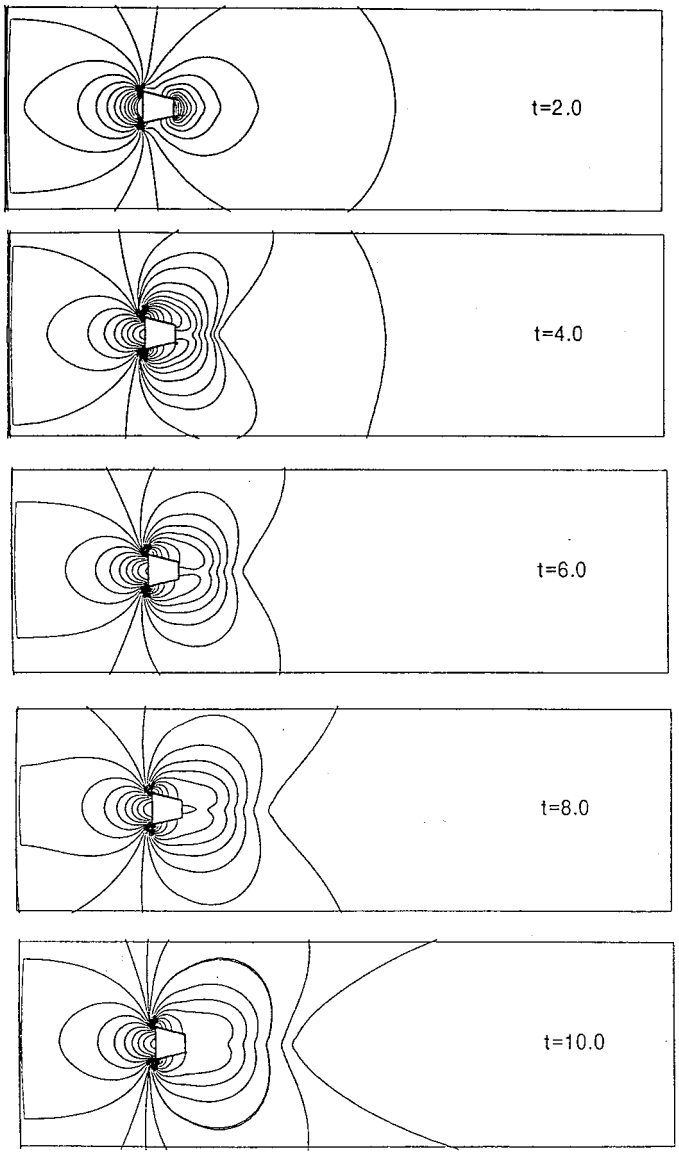

Figure 11. Time variation of the pressure contours at $Re = 50$.

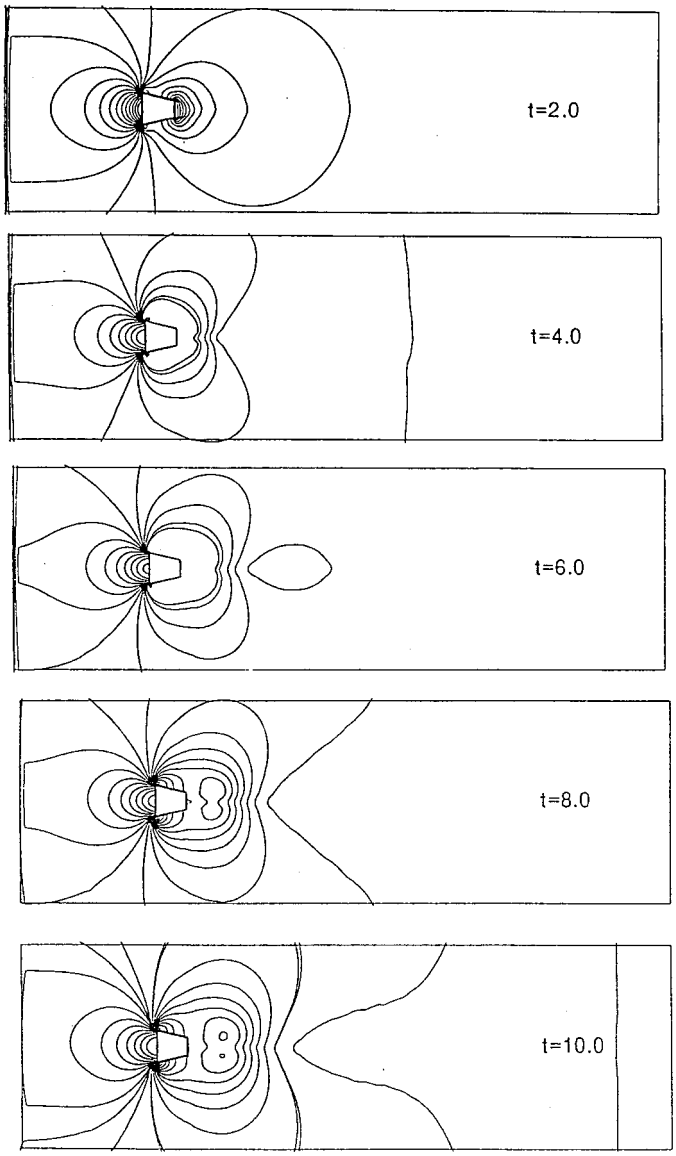

Figure 12. Time variation of the pressure contours at $Re = 150$.

the secondary recirculation region. A longer period of time is required for the drag coefficients to reach steady state values because of the appearance of the secondary recirculation. In general, the higher the Reynolds number, the smaller the Cd steady state value. At the early stages of the impulsively started flow, the drag coefficients decrease more rapidly than after some time intervals. The drag coefficients generally approach a stationary value at large time levels for all the Reynolds numbers considered here.

3.6. Comparisons with available results obtained by other investigators

There have been many studies on separated flow over bluff bodies such as circular cylinders, square cylinders, rectangular cylinders and flat plates. Very few considered the trapezoidal cylinders. However, with the limited numerical and experimental results reported in the literature, the results obtained in the present work compared very well with the available results. For example, the pressure contours obtained by Ling *et al.* [4] are very similar to the present computed pressure contours as shown in Figures 10–15. The drag coefficients of configuration No. 4 of Davis and Moore [1] approach a value of $Cd \approx 1.5$ after a dimensionless

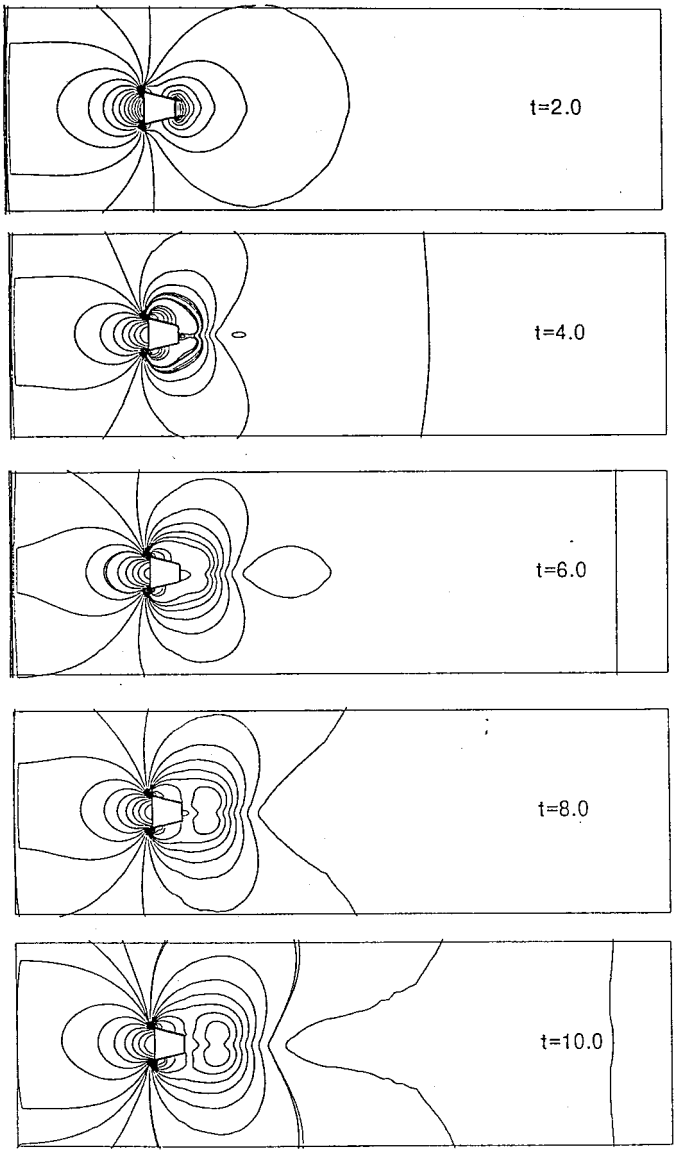

Figure 13. Time variation of the pressure contours at $Re = 250$.

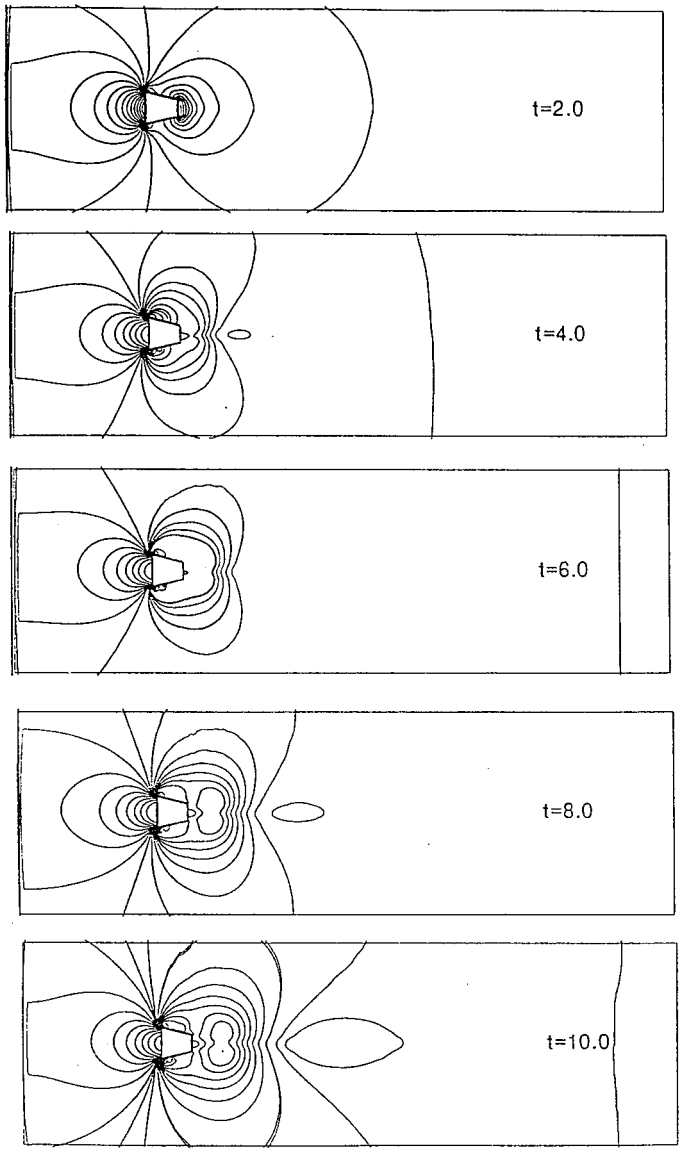

Figure 14. Time variation of the pressure contours at $Re = 500$.

time scale of $t \geq 20$ for higher Reynolds number flow. This is consistent with the results obtained in Figure 19 where $Cd \rightarrow 1.5$ for higher Reynolds numbers in the present study. Wind tunnel tests were also carried out by Lee *et al.* [18] to obtain the drag coefficients of prismatic bodies with trapezoids as the after body shapes. The surface pressure distributions obtained around the trapezoidal cylinders are similar to those shown in Figures 16 and 17. Positive pressure coefficients near the magnitude of 1.0 are always shown on the surfaces facing the approaching flow. Immediately after the frontal surface shape corners, the pressure coefficients drop to extreme negative values. Typical pressure coefficients are in the range of $Cp = -2.0$ to -3.0, after which they recover to some uniform negative values within the wake region.

These experimental results are similar to those shown in Figures 16 and 17. The experimental wake lengths obtained show a similar trend to those in the present study, described in Figure 18. For the trapezoidal cylinders considered here, wind tunnel tests by Lee *et al.* also show a similar steady state value of $Cd \approx 1.5$ for higher Reynolds numbers, as shown in Figure 19.

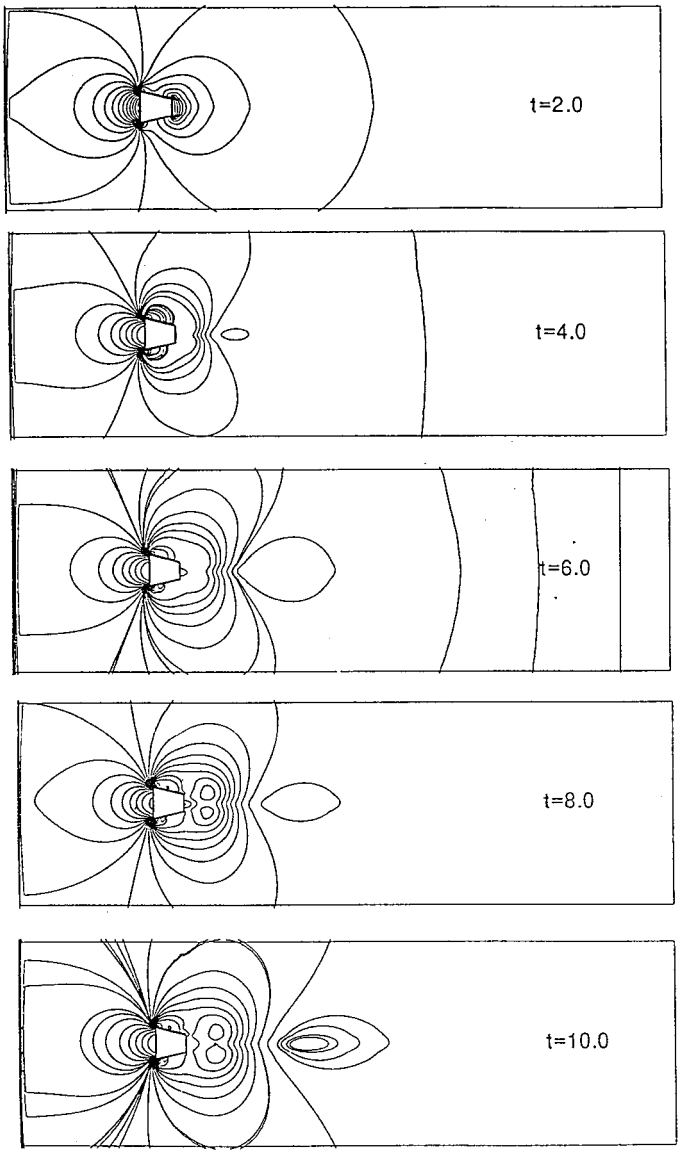

Figure 15. Time variation of the pressure contours at $Re = 1000$.

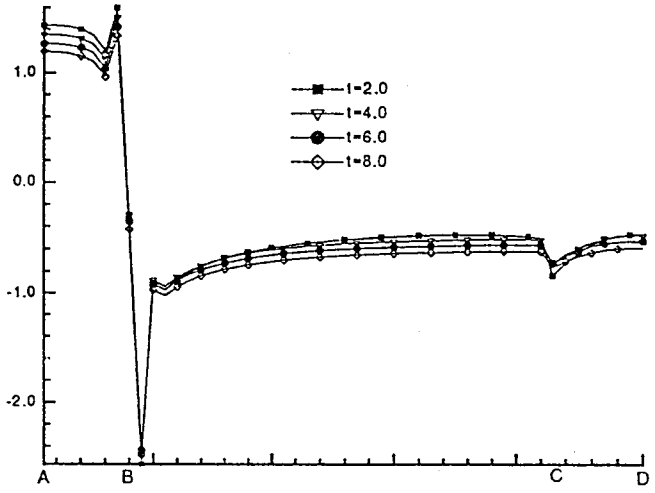

Figure 16. Time variation of the pressure coefficient at $Re = 50$.

4. CONCLUSIONS

Early stages of an impulsively started laminar flow around a tapered trapezoidal cylinder with $25 < Re < 1000$ are studied numerically. The computed results showed that the characteristics of the developing flow recirculation, flow separation, and regimes caused by the interaction of flows are strongly dependent on the approaching Reynolds number. Four main flow regimes have been identified according to whether (i) the flow is predominantly attached to all of the cylinder surfaces (Type I); (ii) flow recirculation develops at the aft end of the cylinder surface (Type II); (iii) flow separation from the leading edges of the cylinder is significant (Type III); (iv) the aft end of the recirculation zone grows and merges with the separating zone of flow from the leading edges; forming a complex tertiary flow phenomenon at the boundary of the

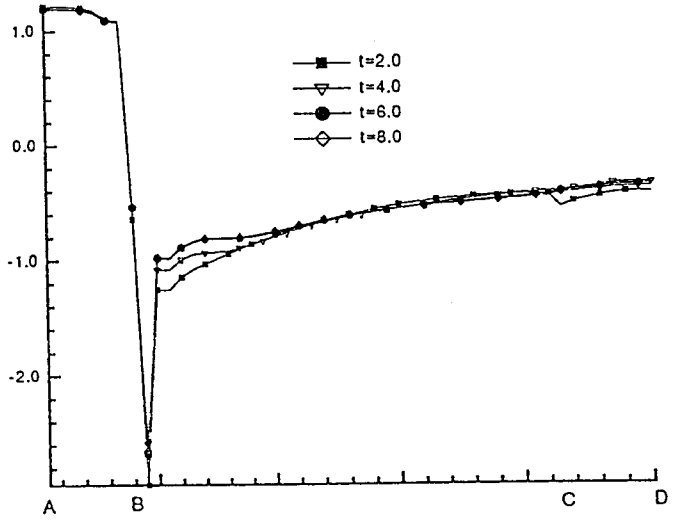

Figure 17. Time variation of the pressure contours at $Re = 500$.

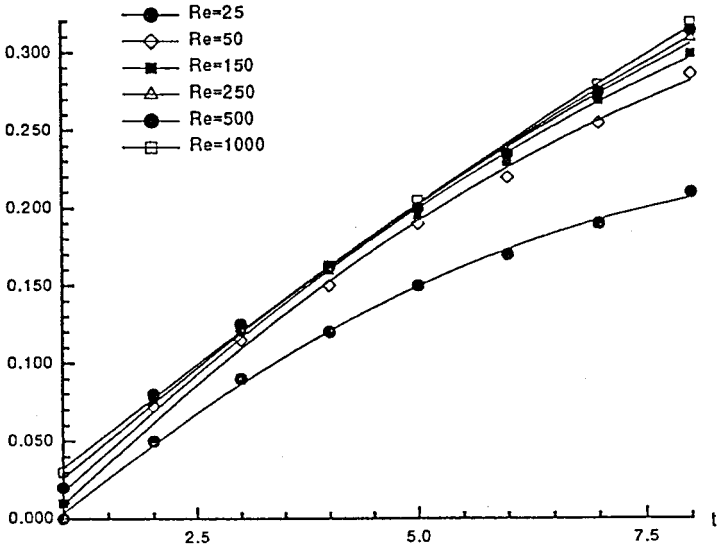

Figure 18. Time variation of the wake length.

two main mixing zones (Type IV). Within the Type I–IV main flow characteristics, three significant subflow regimes were also identified. Subflow (a) shows the growth and development of the symmetrical eddies aft of the cylinder surface; subflow (b) identifies the spreading characteristics of the separating shear layer from the leading edges of the cylinder and the development along the inclined surfaces; and subflow (c) analysed the complex disturbed flow regime near the meeting point between the developing Type II and Type III flows.

For $Re < 25$, the initial flow develops with time, without visible flow separation (Type I). After a short lapse of time, the flow predominantly separates from the rear surface of the

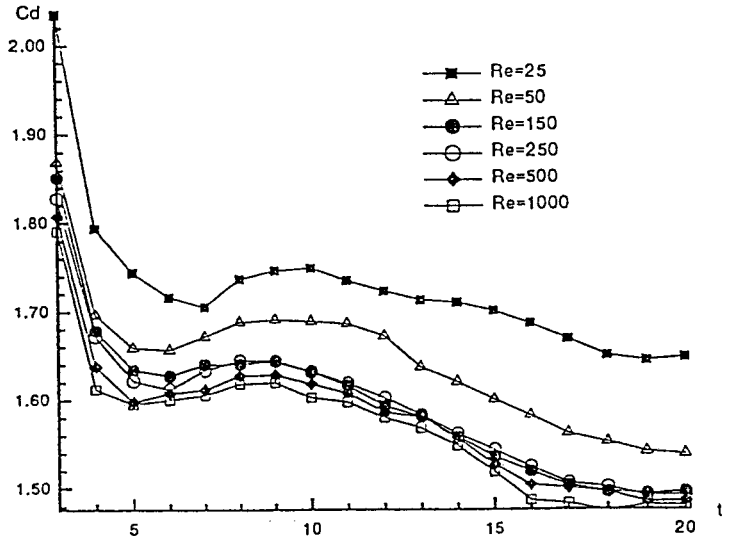

Figure 19. Time variation of the drag coefficients for various *Re*.

square and forms symmetrical eddies within a recirculating zone about the rear axis of the cylinder (Type II). For $25 < Re < 250$, a significant secondary phenomenon was quickly observed, viz. the development of a flow separation on the upper and lower inclined surfaces of the tapered trapezoidal cylinder (Type III). For $Re > 250$, the merging of the separation flow (Type III) from the upper and lower inclined surfaces of the cylinder with the recirculation zone of the wake region (Type II) forming the Type IV flow was observed. For a given Re, once Type II and Type III recirculatory flows merge, the overall recirculation flow of Type IV usually remains fairly constant with the advancement of time.

The time evolution of the various characteristics of the subflow regions occur during different phases of the main flow developments. Initially, the primary recirculatory region aft of the cylinder (subflow (a)) grows with the width of the wake which is less than the width of the aft end of the tapered trapezoidal cylinder. As time advances, subflow (a) grows wider than the width of the square cylinder, and eventually merges with the elongated upper and lower separated surface shear layers (subflow (b)) from the leading edges of the cylinder. When subflows (a) and (b) merge, complex tertiary subflow (c) region develops at the merging point. At this stage, the recirculating zone at the aft end of the cylinder grows wider than the aft width of the cylinder. The length of the separating shear layer from the leading edges grows longer than the length of the cylinder.

Individualization of a rapid vortex source during the very early phase of the flow evolution was also observed. This gives rise to the main eddy, which occurs near the aft end of the cylinder. Subsequently, a rear stagnation point was then formed away from the aft surface of the cylinder. This downstream stagnation point moves rapidly downstream as Re increases and is a measure of the wake length for the flow development. Comparisons with available results obtained by other investigators showed very good agreement.

ACKNOWLEDGMENTS

The author gratefully acknowledges the financial assistance of a research grant RP890633 from the National University of Singapore. During the course of this work, the assistance of Dr S.H. Winoto, Mr Y.P. Xu and Mr Ronald Tan are also gratefully acknowledged.

APPENDIX A. NOMENCLATURE

a	width of the frontal surface of the trapezoidal cylinder
ADI	alternating direction implicit method
b	width of the aft end surface of the trapezoidal cylinder
Cp	pressure coefficient
Cd	drag coefficient
J	Jacobian matrix
L	characteristic length ($L = b$)
p	non-dimensional pressure
Re	Reynolds number ($\rho u_0 \cdot L/\mu$)
t	time
TDMA	tridiagonal matrix algorithm
u_ξ	non-dimensional velocity in the ξ-direction
u_η	non-dimensional velocity in η-direction
U	mean velocity at inlet section, the characteristic velocity

V_{max} maximum non-dimensional velocity
ξ longitudinal co-ordinate in generalized system
η lateral co-ordinate in generalized system
ν fluid molecular kinetic viscosity
ψ streamfunction
ζ vorticity

REFERENCES

1. R.W. Davis and E.F. Moore, 'A numerical study of vortex shedding from rectangles', *J. Fluid Mech.*, **116**, 475–506 (1982).
2. S. Nagano, 'A numerical analysis of two-dimensional flow past a rectangular prism by a discrete cortex model', *Comput. Fluids*, **10**, 243–259 (1982).
3. M.S.U.K. Fernando and V.J. Modi, 'A numerical analysis of unsteady flow past bluff bodies', *Comput. Mech.*, **6**, 11–34 (1990).
4. L.M. Ling, B. Ramaswamy, R.D. Cohen and T.C. Jue, 'Numerical analysis on Strouhal frequencies in vortex shedding over cylinders with surface suction and blowing', *Int. j. numer. methods heat fluid flow*, **3**, 357–375 (1993).
5. S.W. Kim and T.J. Benson, 'Comparison of the SMAC, PICO and ITERATIVE TIME-ADVANCING schemes for unsteady flows', *Int. j. numer. methods fluids*, **21**, 435–454 (1992).
6. P.W. Bearman and D.M. Trueman, 'An investigation of the flow around rectangular cylinders', *Aeronaut. Q.*, **23**, 229–237 (1972).
7. M. Coutanceau and R. Bouard, 'Experimental determination of the main features of the viscous hydrodynamic field in the wake of a circular cylinder in a uniform stream', *J. Fluid Mech.*, **79**, 231–239 (1977).
8. R. Bouard and M. Coutanceau, 'The early stage of development of the wake behind an impulsively started cylinder for $40 < Re < 10^4$', *J. Fluid Mech.*, **101**, 583–607 (1980).
9. J.H. Gerrard, 'The mechanics of the formation region of vortices behind bluff bodies', *J. Fluid Mech.*, **25**, 401–410 (1966).
10. J.H. Gerrard, 'The wakes of cylindrical bluff bodies at low Reynolds number', *Phil. Trans. Roy. Soc. A*, **288**, 29–38 (1978).
11. A. Okajima, 'Strouhal numbers of rectangular cylinders', *J. Fluid Mech.*, **123**, 379–398 (1982).
12. A. Okajima and K. Kitajima, 'Numerical study on wake patterns and aerodynamic forces of an oscillating cylinder with a circular and rectangular cross-section', *J. Wind Eng. Ind. Aerodyn.*, **50**, 39–48 (1993).
13. K. Kyoji and Y. Yoshifumi, 'Observation of the flow around a circular cylinder and a trapezoidal cylinder in a circular pipe by a dye-injection method', *11th Australasian Fluid Mech. Conf.*, 14–18 Dec 1992, Vol. 1, 201–207 (1992).
14. A.A. Samarskii and V.B. Andree, 'On the high accuracy difference scheme for an elliptic equation with several space variables', *USSR Comput. Math. Phys.*, **3**, 1373–1382 (1963).
15. P.J. Roache, *Computational Fluid Dynamics*, Hermosa, 1972.
16. T.S. Lee, R.S. Tan and X.P. Xu, 'Numerical study of an impulsively started laminar fluid flow over a square cylinder', *Int. j. numer. methods heat fluid flow*, **6**, 53–70 (1996).
17. P.K. Khosla and S.G. Rubin, 'Diagonally dominant second-order accurate implicit scheme', *Comput. Fluids*, **2**, 207–209 (1974).
18. T.S. Lee, S.C. Luo, Y.T. Chew and M.G. Yazdani, 'Galloping of prismatic bodies with different afterbody shapes', *Proc. 4th Int. Offshore and Polar Engineering Conference (ISOPE'94)*, 10–15 April 1994, Osaka, Japan, pp. 364–369.

